

properties from the emission in the outer or 'conal' regions. Polarization observations of this pulsar<sup>14</sup> at 659 MHz show that the pulse is weakly polarized with a very rapid swing of position angle through the pulse. This, and the narrow and nearly gaussian pulse profile, suggests that the entire observed pulse is core-type emission with the beam direction close to that of the magnetic axis.

We note that the period of PSR J2144–3933 is similar to the periods of anomalous X-ray pulsars<sup>15</sup> (AXPs) and pulsars identified with soft  $\gamma$ -ray repeaters<sup>16</sup> (SGRs). These slowly spinning neutron stars have been interpreted as 'magnetars', whose emission is powered not by the rotational kinetic energy of the neutron star, but by the decay of its super-strong magnetic field<sup>17</sup>. No AXPs or SGRs have yet been detected as radio pulsars, and it has been argued that such pulsars may not emit in the radio band because photon splitting inhibits pair-production<sup>18</sup>. However, we note that the lack of detection of radio emission from the few known AXPs and SGRs can be explained if their radio beamwidths are similar to that of PSR J2144–3933; if this were so, only a very small fraction of the total population of such objects would be visible from Earth as radio pulsars. The surface magnetic field of PSR J2144–3933 itself is much less than that of magnetars, and no magnetar-like X-ray emission would be expected from this object.

For a given magnetic field configuration, the locus of  $P$ – $B_s$  values at which radio emission ceases defines a 'death line' in the  $P$ – $B_s$  diagram (Fig. 2), to the right of which no pulsar should emit radio waves. By invoking a variety of assumptions about field-line curvature in the emission region above the neutron star, Chen and Ruderman<sup>19</sup> derived a set of death lines. For a given surface magnetic dipole field strength, pulsars with strong multipolar field components will have a highly curved field near the stellar surface permitting the emission to persist to longer periods. In Fig. 2, death line B corresponds to the greatest reasonable magnetic field curvature, and death line C is an extreme and unlikely case. No pulsar should exist with a surface magnetic dipole field strength and period which place it to the right of these death lines. PSR J2144–3933 lies to the right of both lines. It is (to our knowledge) the first pulsar known to do so, and calls into question the assumptions made in deriving the death lines.

One possibility is that the neutron-star properties might differ from those commonly assumed. For example, the derived value of  $B_s$  is proportional to  $(I/R^6)^{1/2}$ , where  $I$  and  $R$  are the neutron-star moments of inertia and radius, respectively<sup>5</sup>. For different equations of state,  $I/R^6$  may vary by up to two orders of magnitude. If PSR J2144–3933 has a larger-than-average value of  $I/R^6$ , the magnetic dipole field strength may be large enough to permit pair production and hence radio emission.

Alternatively, it may be that the radio emission process does not depend on pair-production. Weatherall and Eilek<sup>20</sup> have suggested that pulsars lying below line A (Fig. 2) all have conal properties, whereas most of those above it are dominated by core emission; they also suggested that conal emission may be generated by a mechanism not dependent on pair production. PSR J2144–3933 has clear signatures of core emission, and the presence of this pulsar beyond death line A is inconsistent with the hypothesis of Weatherall and Eilek. We note that PSR J1951+1123 also lies well below this death line and has a very narrow pulse, consistent with expectations for core emission<sup>10,12</sup>. We suggest that the fact that few core-dominated pulsars are seen beyond death line A is just a selection effect due to the narrow beamwidth of the core emission.

PSR J2144–3933 has the lowest spindown luminosity ( $\sim 3 \times 10^{28}$  ergs<sup>-1</sup>) of any known pulsar. It is also relatively nearby—the distance,  $d$ , estimated from the dispersion measure<sup>8,21</sup> is only  $\sim 180$  pc—and so its radio luminosity,  $L_{400}$ , is low;  $L_{400} = S_{400} d^2 \approx 0.13$  mJy kpc<sup>2</sup>, where  $S_{400}$  is its mean flux density at 400 MHz. If the beam is assumed to be circular, the beaming fraction (that is, the fraction of the celestial sphere swept across by the beam) is also extremely small,  $\sim 0.01$ . Its low luminosity and

the very low beaming fraction together imply that we can observe only a very small proportion of the total population of such objects in the Galaxy. While extrapolation from the detection of a single object is always uncertain (some would say foolhardy), there is no reason to suppose that PSR J2144–3933 is unique. With this caveat, this detection implies a Galactic population of similar pulsars of the order of  $10^5$ , comparable to previous estimates of the size of the total pulsar population<sup>22,23</sup>. □

Received 23 March; accepted 13 July 1999.

1. Ruderman, M. A. & Sutherland, P. G. Theory of pulsars: Polar gaps, sparks, and coherent microwave radiation. *Astrophys. J.* **196**, 51–72 (1975).
2. Machabeli, G. Z. & Usov, V. V. Cyclotron instability in the magnetosphere of the Crab Nebula pulsar, and the origin of its radiation. *Sov. Astron. Lett.* **5**, 238–241 (1979).
3. Cheng, A. F. & Ruderman, M. A. Particle acceleration and radio emission above pulsar polar caps. *Astrophys. J.* **235**, 576–586 (1980).
4. Beskin, V. S., Gurevich, A. V. & Istomin, Y. N. Theory of the radio emission of pulsars. *Astrophys. Space Sci.* **146**, 205–281 (1988).
5. Manchester, R. N. & Taylor, J. H. *Pulsars* (Freeman, San Francisco, 1977).
6. Manchester, R. N. *et al.* The Parkes Southern Pulsar Survey—I. Observing and data analysis systems and initial results. *Mon. Not. R. Astron. Soc.* **279**, 1235–1250 (1996).
7. Lyne, A. G. *et al.* The Parkes Southern Pulsar Survey—II. Final results and population analysis. *Mon. Not. R. Astron. Soc.* **295**, 743–755 (1998).
8. D'Amico, N. *et al.* The Parkes Southern Pulsar Survey—III. Timing of long-period pulsars. *Mon. Not. R. Astron. Soc.* **297**, 28–40 (1998).
9. Johnston, S., Nicastro, L. & Koribalski, B. Scintillation parameters for 49 pulsars. *Mon. Not. R. Astron. Soc.* **297**, 108–116 (1998).
10. Camilo, F. & Nice, D. J. Timing parameters of 29 pulsars. *Astrophys. J.* **445**, 756–761 (1995).
11. Lyne, A. G. & Manchester, R. N. The shape of pulsar radio beams. *Mon. Not. R. Astron. Soc.* **234**, 477–508 (1988).
12. Rankin, J. M. Toward an empirical theory of pulsar emission. IV. Geometry of the core emission region. *Astrophys. J.* **352**, 247–257 (1990).
13. Rankin, J. M. Toward an empirical theory of pulsar emission. I. Morphological taxonomy. *Astrophys. J.* **274**, 333–358 (1983).
14. Manchester, R. N., Han, J. L. & Qiao, G. J. Polarization observations of 66 southern pulsars. *Mon. Not. R. Astron. Soc.* **295**, 280–298 (1998).
15. van Paradijs, J., Taam, R. E. & van den Heuvel, E. P. J. On the nature of the 'anomalous' 6-s X-ray pulsars. *Astron. Astrophys.* **299**, L41–L44 (1995).
16. Kouveliotou, C. *et al.* An X-ray pulsar with a superstrong magnetic field in the soft  $\gamma$ -ray repeater SGR1806–20. *Nature* **393**, 235–237 (1998).
17. Duncan, R. C. & Thompson, C. Formation of very strongly magnetized neutron stars: Implications for gamma-ray bursts. *Astrophys. J.* **392**, L9–L13 (1992).
18. Baring, M. G. & Harding, A. K. Radio-quiet pulsars with ultra-strong magnetic fields. *Astrophys. J.* **507**, L55–L58 (1998).
19. Chen, K. & Ruderman, M. Pulsar death lines and death valley. *Astrophys. J.* **402**, 264–270 (1993).
20. Weatherall, J. C. & Eilek, J. A. Are there two pulsar emission mechanisms? *Astrophys. J.* **474**, 407–413 (1997).
21. Taylor, J. H. & Cordes, J. M. Pulsar distances and the Galactic distribution of free electrons. *Astrophys. J.* **411**, 674–684 (1993).
22. Lyne, A. G., Manchester, R. N. & Taylor, J. H. The Galactic population of pulsars. *Mon. Not. R. Astron. Soc.* **213**, 613–639 (1985).
23. Lorimer, D. R., Bailes, M., Dewey, R. J. & Harrison, P. A. Pulsar statistics: The birthrate and initial spin periods of radio pulsars. *Mon. Not. R. Astron. Soc.* **263**, 403–415 (1993).
24. Tauris, T. M. & Manchester, R. N. On the evolution of pulsar beams. *Mon. Not. R. Astron. Soc.* **298**, 625–636 (1998).

**Acknowledgements.** M.D.Y. thanks R. Burman for comments on this manuscript, and R. Burman and B. Kenny for advice. M.D.Y. also thanks the University of Western Australia for partial financial support. The Parkes radio telescope is part of the Australia Telescope, which is funded by the Commonwealth of Australia for operation as a National Facility managed by CSIRO.

Correspondence and requests for materials should be addressed to M.D.Y. (e-mail: matthew@physics.uwa.edu.au).

## Measurement of gravitational acceleration by dropping atoms

Achim Peters, Keng Yeow Chung & Steven Chu

Physics Department, Stanford University, Stanford, California 94305-4060, USA

**Laser-cooling of atoms and atom-trapping are finding increasing application in many areas of science<sup>1</sup>. One important use of laser-cooled atoms is in atom interferometers<sup>2</sup>. In these devices, an atom is placed into a superposition of two or more spatially separated atomic states; these states are each described by a quantum-mechanical phase term, which will interfere with one another if they are brought back together at a later time. Atom**

interferometers have been shown to be very precise inertial sensors for acceleration<sup>3,4</sup>, rotation<sup>5</sup> and for the measurement of the fine structure constant<sup>6</sup>. Here we use an atom interferometer based on a fountain of laser-cooled atoms to measure  $g$ , the acceleration of gravity. Through detailed investigation and elimination of systematic effects that may affect the accuracy of the measurement, we achieve an absolute uncertainty of  $\Delta g/g \approx 3 \times 10^{-9}$ , representing a million-fold increase in absolute accuracy compared with previous atom-interferometer experiments<sup>7</sup>. We also compare our measurement with the value of  $g$  obtained at the same laboratory site using a Michelson interferometer gravimeter (a modern equivalent of Galileo's 'leaning tower' experiment in Pisa). We show that the macroscopic glass object used in this instrument falls with the same acceleration, to within 7 parts in  $10^9$ , as a quantum-mechanical caesium atom.

Here we focus on extending the precision of atom interferometers by increasing the interferometer measurement time with the use of an atomic fountain of laser-cooled atoms and by using atom optics components based on optical pulses of light. We have shown<sup>4</sup> how an atom interferometer may be used to measure  $g$  with a precision of 1 part in  $10^{10}$ . The absolute relative uncertainty  $\Delta g/g$  of 3 parts in  $10^9$  achieved in the current work demonstrates that this type of atom interferometer can be used to make absolute measurements comparable with the most sensitive measurement tools in physics. We believe that this work is also the best confirmation of the equivalence principle between a quantum and macroscopic object. By comparison, there still remains a discrepancy of a few per cent between  $g$  measured by neutron interferometry and a macroscopic object<sup>8</sup>, and we may conclude that there are aspects of neutron interferometry that are not well understood. Finally, the high fringe contrast seen in this interferometer places severe constraints on speculations concerning the possibility of quantum-state phase diffusion due to space-time fluctuations<sup>9</sup>.

Our atom interferometer uses optical pulses of light to stimulate transitions between two different states of the atoms. The atoms are first exposed to an optical ' $\pi/2$ -pulse' defined as a pulse of light that puts an atom initially in the state  $|1, p\rangle$ , characterized by an internal state  $|1\rangle$  and momentum  $p$ , into an equal superposition of the original state  $|1, p\rangle$  and a second state; this second state is characterized by an internal state  $|2\rangle$  and momentum  $p + \hbar k$ , and is denoted

by  $|2, p + \hbar k\rangle$ . Here,  $\hbar k$  is the momentum imparted by the optical pulse. After a time  $T$ , the two parts of the atom drift apart by a distance  $\hbar k T/M$ , where  $M$  is the mass of the atom. Excitation by a so-called ' $\pi$ -pulse' induces the part of the atom in state  $|1, p\rangle$  to make the transition  $|1, p\rangle \rightarrow |2, p + \hbar k\rangle$  and the part of the atom in  $|2, p + \hbar k\rangle$  to make the transition  $|2, p + \hbar k\rangle \rightarrow |1, p\rangle$ . After another time  $T$ , the two parts of the atom come back together and a second  $\pi/2$ -pulse with the appropriate phase relative to the atomic phase can put the atom into either of the states  $|1, p\rangle$  or  $|2, p + \hbar k\rangle$ . Earlier analysis<sup>3</sup> has shown that the phase difference between the two paths of the interferometer is given by

$$\Delta\Phi = (\Phi_1(t_1) - \Phi_2(t_2))_{\Gamma_1} - (\Phi_2(t_2) - \Phi_3(t_3))_{\Gamma_2}$$

where  $\Phi_i(t_i) = kz_i - \omega t_i$  are the phases of the laser light at positions  $z_i$  and times  $t_i$  at the beginning of each optical pulse,  $\omega$  is the frequency of the light, and  $\Gamma_i$  denotes the two classical paths. In our experiment, the frequency of the light is changed in a phase-continuous way, so that it remains resonant with the transition  $|1, p\rangle \rightarrow |2, p + \hbar k\rangle$  as the atom accelerates owing to gravity. Under these conditions, we have shown<sup>3</sup> that  $\Delta\Phi = kgT^2$ .

The internal states used in the experiment are the two magnetic-field-insensitive hyperfine ground states of caesium. Counter-propagating laser beams induce two-photon Raman transitions between these states, which doubles the mechanical effect of a single-photon transition. More importantly, the optical transition is determined by the frequency difference of two laser beams which is phase-locked to a stable microwave source. Thus, we have precise control of the frequency and the phase of the light.

We have analysed the complications due to gravity. The lowest-order correction to  $g$  for a constant gravity gradient  $\gamma$  is

$$\Delta g = \gamma \left( \frac{7}{12} g_0 T^2 - v_0 - z_0 \right)$$

where  $z_0$  and  $v_0$  are the position and velocity of the atom referenced to a point in the laboratory free of vibrations just before the first  $\pi/2$ -pulse<sup>10</sup>. In our laboratory,  $\gamma \approx 3 \times 10^{-7} \text{ g m}^{-1}$ , due mostly to the gradient of the Earth's gravitational field. For typical experimental parameters, the gradient correction is 31 parts per billion (p.p.b.)

The experimental set-up is shown in Fig. 1. About  $5 \times 10^8$  caesium atoms are extracted from a low-pressure background vapour and loaded into a magneto-optic trap (MOT) in 600 ms. After turning off the magnetic fields, the atoms are launched using moving polarization gradient optical molasses<sup>11</sup>. During this time,

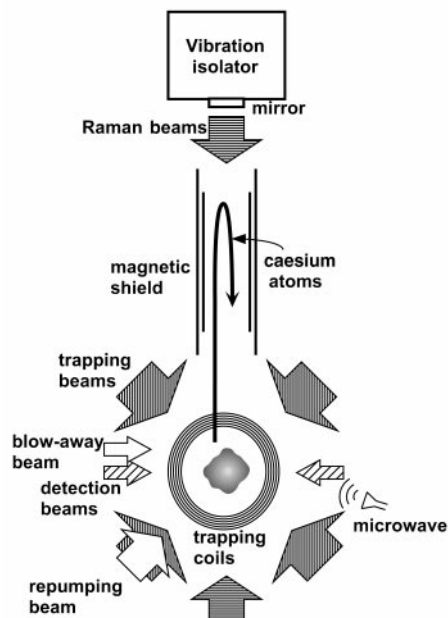


Figure 1 Overview of the experimental set-up.

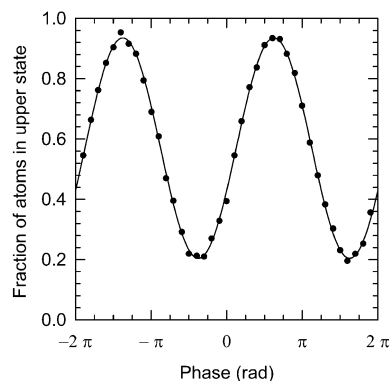


Figure 2 Typical Doppler-sensitive interferometer fringe for  $T = 160$  ms. Shown are the 588,638th and 588,639th fringes. Each of the 40 data points represents a single launch of the atoms, spaced 1.3 s apart and taken over a period of 1 min. One full fringe corresponds to  $\sim 2 \times 10^6 g$ . Performing a least-squares fit determines local gravity to approximately  $3 \times 10^{-9} g$ .

the atoms are further cooled by tuning the molasses beams 60 MHz below resonance and lowering the intensity to  $5 \text{ mW cm}^{-2}$ . In the final stages of the launch, laser intensities are decreased to zero in  $400 \mu\text{s}$  so that the atoms are also adiabatically cooled<sup>12</sup>. The final temperature of the launched atoms is  $\sim 1.5 \mu\text{K}$ .

The launched atoms are subjected to a sequence of pulses (microwave, velocity-selective Raman, and state-selective blow-away) that places  $3 \times 10^6$  atoms in the  $6S_{1/2}$ ,  $F = 3$ ,  $m_F = 0$  state with an effective vertical temperature of 10 nK. This low velocity spread gives us a fringe contrast of  $\sim 65\%$  for all times  $T$  between 0.5 and 160 ms.

The interferometer measurement occurs in a magnetically shielded region. The optical pulses are derived from two external-cavity phase-locked diode lasers. Different polarization configurations and intensities have been used throughout the experiment without affecting the accuracy or sensitivity of the measured  $g$ , within our experimental relative uncertainty of 2 p.p.b. The Raman difference frequency is controlled by a direct digital frequency synthesizer which is referenced to a Loran-C frequency standard. The frequency difference is switched between three fixed frequencies to compensate for the gravity-induced Doppler shift during the 320-ms interferometer free-fall time<sup>10</sup>.

Both Raman beams enter the vacuum chamber from below and are retro-reflected (Fig. 1). As the atomic transitions are Doppler sensitive, only one beam from each pair of upward- and downward-travelling beams is in resonance with the atoms. Because the two Raman beams travel over a common path before entering the vacuum system, laboratory vibrations frequency-shift the two beams by nearly the same amount. Thus, only vibrations of the

**Table 1 Known noise sources**

Noise source	$\sigma_g$ (p.p.b.)
Atom shot noise	0.16
Intensity and frequency fluctuation of detection laser	0.9
Loran-C frequency stability	3.0
Raman-laser intensity noise	3.5
Residual vibrations	5
Fluctuation of fluorescence with no MOT atoms	7
Phase noise of 9.2-GHz source	11
Overall known noise sources	15
Observed noise	19

Known noise sources and their estimated effect on a gravity measurement with  $T = 160$  ms between interferometer pulses of lengths  $\tau_r = 80 \mu\text{s}$  and  $\tau_{\text{avg}} = 40 \mu\text{s}$ .  $\sigma_g$  denotes the standard deviation of a set of 40 measurements. If the actual vibration noise of the platform is a factor of 2 higher than noise calculated from the error signal, we have a full accounting of the observed noise.

retro-mirror affect the Raman difference frequency. This mirror is mounted on an actively stabilized, vibration isolation system. The acceleration, measured by a low-noise, low-frequency force feedback accelerometer (CMG-3V, Guralp, Reading, UK), is digitized and processed. An output signal is then used to control the current through a solenoid actuator. The platform has an effective resonance of 0.02 Hz and reduces vibrations between 0.2 to 5 Hz by two orders of magnitude<sup>13</sup>. Without this vibration isolation, our interference fringes vanish for  $T$  greater than  $\sim 40$  ms. With the feedback circuit on, there is essentially no loss of fringe contrast up to the maximum drop times, limited by the size of the magnetically shielded region. Further motion control in our apparatus includes an active tilt control to maintain the tilt of the retro-mirror to within  $10 \mu\text{rad}$ . Rotations of the optical table about the horizontal axes are reduced through three one-dimensional active feedback vibration isolators placed at three corners of the table.

Typical interferometer data for a pulse spacing of  $T = 160$  ms are shown in Fig. 2. One minute of integration time allows us to determine  $g$  with a precision of  $3 \times 10^{-9} g$ . To locate the central fringe, we vary  $T$  from 2 to 160 ms. Figure 3a shows a continuous measurement of  $g$  over a period of 3 days, with each dot corresponding to data similar to Fig. 2. Figure 3b shows the difference between our measurement and two tidal models<sup>14</sup>. The tidal model that included the ocean loading<sup>15</sup> effect on our local environment is found to agree with our data with a precision of  $1 \times 10^{-10} g$  after two days of integration time.

During the course of our experiment, we have arranged for an absolute gravimeter<sup>16</sup> (FG-S, Micro-g Solutions, Arvada, Colorado), to be run in our laboratory for three days to measure the absolute value of  $g$ . This is a Michelson optical interferometer with one arm defined by a freely falling corner-cube and has a quoted relative uncertainty of 2 p.p.b. A comparison with the value of  $g$  we obtained in a 2-day run shows a difference of  $(7 \pm 7)$  p.p.b. This comparison was limited mostly by a 5-p.p.b. uncertainty in our measurement of the local gravity gradient, which produces a 3 p.p.b. correction per cm vertical displacement. The two instruments were separated by 2 metres in our laboratory with a 0.5-m height difference.

Direct comparison of the noise of both instruments also showed that our atom interferometer has a 4 times higher resolution than the falling-corner-cube gravimeter, mainly due to the slower FG5 repetition rate (1/15 Hz) compared with our instrument (1/1.3 Hz). The noise per launch for both instruments was similar.

The use of an active low-frequency vibration isolator overcomes the main limitation of the previous  $g$  experiment. With a well supported vibration isolator enclosed in an acoustic isolation box and proper alignment of all the components of the system with the atoms, the noise due to vibrations, calculated from an integration of the power spectral density of the noise and the frequency-dependent system response, was found to be 5 p.p.b. This is lower than some of the other main noise sources (Table 1). With better frequency

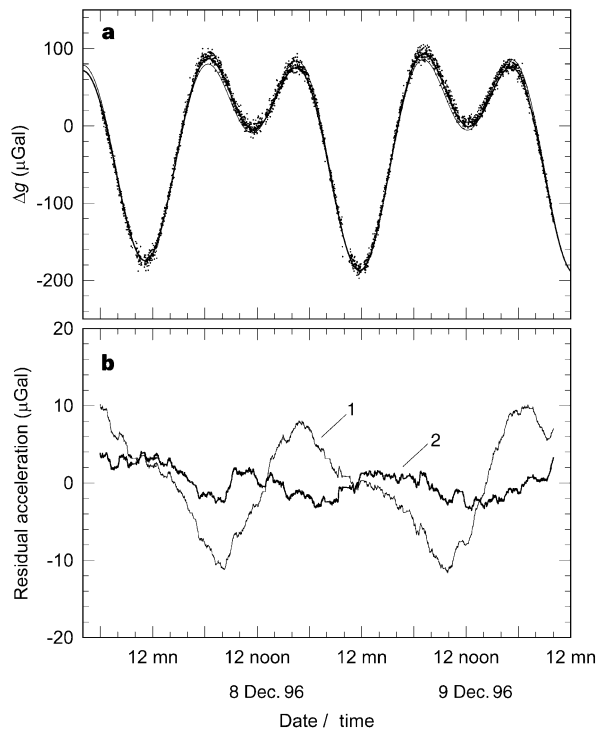


**Figure 3** Comparison between experimental data and tide models. **a**, A closer look at two days of gravity data. Each data point represents a one-minute gravity measurement. The solid lines represent two different tidal models.  $1 \mu\text{Gal} = 10^{-8} \text{ m s}^{-2} \approx 10^{-9} g$ . **b**, the residuals of the data with respect to a tidal model where (trace 1) the Earth is modelled as a solid elastic object and where (trace 2) the effects of ocean loading of the Earth are taken into account. Data for ocean loading were provided by H.-G. Scherneck. Effects at the few p.p.b. level, such as changes in the local barometric pressure, have not been included.

**Table 2 The main known potential systematic effects**

	Relative uncertainty (p.p.b.)
Systematic error	
Cs wavelength	0.3
Laser lock offset	0.4
r.f. phase shift	2
Coriolis effect	2
Gravity gradient	0.2
a.c. Stark shift	1
Dependence on pulse timing	1
Overall instrumental uncertainty	3.2
Environmental effect	
Pressure correction	1
Ocean loading	1
Other environmental effects	2

Systematic effects that are  $\leq 0.1$  p.p.b. are not listed: these include possible effects of magnetic field gradients. The environmental effects are important in comparing values of  $g$  obtained at different times. Other environmental effects include water-table correction.

sources, active stabilization of the intensity of the Raman beams, and moving the detection region away from the caesium beam, these main noises could be reduced to less than 1 p.p.b. Further investigation of an artificial noise floor of the vibration isolator system could bring the eventual performance of the instrument to within a factor of 10 of the shot-noise limit.

Table 2 shows the most important systematic effects that we have identified, and their associated uncertainties. Other effects, such as magnetic-field gradients, wavefront curvature, speckle, dispersion in the air and windows, timing and switching errors in the optical pulses, were experimentally found to be below the 0.1-p.p.b. level and are not listed. We have also estimated relativistic corrections ( $< 0.1$  p.p.b.) and the effect of a changing effective wavevector due to different propagation delays during the interferometer sequence (corrected to an uncertainty of  $< 0.1$  p.p.b.). We now consider the possible contributions of other potential sources of instrumental uncertainty.

Dynamical diffraction treatment in neutron interferometer experiments corrected the original measurement of  $g$  by a few per cent (ref. 8). Borde pointed out that a similar effect is also present in our experiment, and should depend on the detuning of the laser from the atomic resonance caused by gravitational acceleration during the pulse<sup>17</sup>. Experimentally, we found no difference (within the experimental uncertainty of 2 p.p.b.) whether the detuning was always kept at zero by chirping the pulse to account for the acceleration due to gravity or whether detuning was zero only at the middle of the pulse. Furthermore, the effect of a common detuning on all three pulses was measured to be 1.3 p.p.b. for every Kilohertz detuning from the resonance condition. As the detuning in our experiment is less than 100 Hz, we estimate that this effect should be less than 1 p.p.b. for our experiment.

The light pulses could potentially induce a.c. Stark shifts and lead to systematic error. We measure the a.c. Stark shift by introducing an off-resonance Raman pulse that does not induce transitions in the time between the interferometer  $\pi/2$  and  $\pi$ -pulses. This shift can be made less than 1 p.p.b. by adjusting the ratio of the Raman beam intensities. However, as this ratio tends to fluctuate during the long runs, we assign a 1 p.p.b. uncertainty to this effect.

Coriolis effects occur when atoms have a horizontal velocity. In this case, the photon recoils during the interferometer pulses are not parallel to the atomic velocity, and cause the atom interferometer to enclose a spatial area. The resulting sensitivity to rotation shifts the measured gravity by  $\Delta g = 2\Omega \cdot (\mathbf{v}_0 \times \hat{\mathbf{k}})$ , where  $\Omega$  is the angular rotation,  $\mathbf{v}_0$  is the velocity of the atom and  $\hat{\mathbf{k}}$  is the direction of the photon recoil. At the latitude of our laboratory,  $37.4^\circ$  N, the Earth's rotation of  $7.25 \times 10^{-5}$  rad  $s^{-1}$  would thus cause a 1 p.p.b. shift in  $g$  for atoms that have a velocity of 0.0087 cm  $s^{-1}$  in the east-

west direction, which is small compared to the typical velocity spread of the atomic cloud ( $\sim 1.5$  cm  $s^{-1}$ ). This effect can be reduced to zero if we choose a detection region that equalizes the number of atoms falling to the east and west. By rocking the laser table, and thereby introducing large rotations, we are able to locate this position to within 0.01 cm, resulting in a relative uncertainty of 2 p.p.b. in  $g$ .

Nonlinear frequency-dependent phase shifts in the radio-frequency system controlling the Raman difference frequency mimic a gravity signal. We have substantially reduced this effect by correcting for measured phase shifts, and by averaging results for different directions of  $\mathbf{k}$ . However, these procedures are difficult, and the remaining relative uncertainty of 2 p.p.b. is still one of the leading systematic effects.

We have measured the gravity gradient in the interaction region by launching the atoms to progressively lower heights using  $T = 90$  ms fringes to stay within the magnetically shielded region. The values of  $g$  at different heights show that the gradient is constant and equal to the free-air gradient. This justifies the use of the formula assuming a constant gradient.

We have varied the time of the  $\pi/2 - \pi - \pi/2$  pulses relative to the time of the launch. We observe a variation in  $g$  that quantitatively agrees with a calculated change due to the gravity gradient and the change in the magnitude of the  $k$ -vectors of the light. The fit of our data to the calculated curve (residual  $\approx 1$  p.p.b.) allows us to set an upper limit to a systematic effect due to any 'trajectory effect'.

At p.p.b. levels, uncertainties due to environmental effects become significant. The main uncertainties are listed in Table 2. However, these effects are not part of the instrumental uncertainty.

The measurement that we report here represents a million-fold increase in absolute accuracy compared to measurements obtained by previous atom interferometers. From our study of the systematic effects of our measurement, we consider that further improvements in the control of Coriolis effect—by, for example, rotating the whole system—and ensuring that there is no synchronized noise in the vibration isolator should lead to a relative uncertainty of the order of one part in  $10^{10}$ . □

Received 4 May; accepted 30 June 1999.

1. Chu, S., Cohen-Tannoudji, C. & Phillips, W. D. Nobel lectures in physics 1997. *Rev. Mod. Phys.* **70**, 685–741 (1998).
2. Berman, P. R. (ed.) *Atom Interferometry* (Academic, Chestnut Hill, 1997).
3. Kasevich, M. & Chu, S. Measurement of the gravitational acceleration of an atom with a light pulse atom interferometer. *Appl. Phys. B* **54**, 321–332 (1992).
4. Peters, A., Chung, K. Y., Young, B., Hensley, J. & Chu, S. Precision atom interferometry. *Phil. Trans. R. Soc. Lond. A* **355**, 2223–2234 (1997).
5. Gustavson, T. L., Bouyer, P. & Kasevich, M. Precision rotation measurements with an atom interferometer gyroscope. *Phys. Rev. Lett.* **78**, 2046–2049 (1997).
6. Young, B. *A measurement of fine-structure constant using atom interferometry*. Thesis, Stanford Univ. (1997).
7. Ekstrom, C. R., Schmiedmayer, J., Chapman, M. S., Hammond, T. D. & Pritchard, D. E. Measurement of electric polarizability of sodium with an atom interferometer. *Phys. Rev. A* **51**, 3883–3888 (1995).
8. Werner, S. A. Quantum phase shifts induced by gravity and rotation. *J. Phys. Soc. Jpn* **A** **65**, 51–59 (1997).
9. Percival, I. & Strunz, W. Detection of space-time fluctuations by a model matter interferometer. *Proc. R. Soc. Lond. A* **453**, 431–446 (1997).
10. Peters, A. *High precision gravity measurements using atom interferometry*. Thesis, Stanford Univ. (1998).
11. Weiss, D. S., Riis, E., Kasevich, M., Moler, K. A. & Chu, S. in *Light Induced Kinetic Effects on Atoms, Ions and Molecules* (eds Moi, I., Gozzini, S., Gabbanini, C., Arimondo, E. & Strumia, F.) 35–44 (ETS Editrice, Pisa, 1991).
12. Kastberg, A., Phillips, W. D., Rolston, S. L., Spreew, R. J. C. & Jessen, P. Adiabatic cooling of cesium to 700 nK in an optical lattice. *Phys. Rev. Lett.* **74**, 1542–1545 (1995).
13. Hensley, J. M., Peters, A. & Chu, S. Active low frequency vertical vibration isolation. *Rev. Sci. Instrum.* **70**, 2735–2741 (1999).
14. Melchior, P. J. *The Tides of Planet Earth* (Pergamon, Oxford, 1983).
15. Scherneck, H. G. A parameterized solid Earth tide model and ocean tide loading effects for global geodetic baseline measurements. *Geophys. J. Int.* **106**, 677–694 (1991).
16. Niebauer, T. N., Sasagawa, G., Faller, J. & Hill, R. A new generation of absolute gravimeters. *Metrologia* **32**, 159–180 (1995).
17. Borde, C. J. in *Atom Interferometry* (ed. Berman, P. R.) 257–292 (Academic, Chestnut Hill, 1997).

**Acknowledgements.** We thank G. Sasagawa, H. G. Scherneck, J. Goodkind, M. McWilliams and R. Jachens for helping in the geophysical aspects of this work. K.Y.C. was supported by the National University of Singapore. This work is supported in part by the NSF and the AFOSR.

Correspondence and requests for materials should be addressed to S.C. (e-mail: schu@leland.Stanford.EDU).